



1 **Chromatography related performance of the Monitor for AeRosols and Gases in ambient**
2 **air (MARGA): laboratory and field based evaluation**

3 Xi Chen¹, John T. Walker^{1,*} and Chris Geron¹

4 ¹National Risk Management Research Laboratory, Office of Research and Development, U.S.
5 Environmental Protection Agency, Research Triangle Park, North Carolina, 27711, U.S.A.

6 *Corresponding Author: Tel.:+1 919 541 2288. Email:Walker.JohnT@epa.gov.

7 **Abstract**

8 Evaluation of the semi-continuous Monitor for AeRosols and Gases in ambient air
9 (MARGA, Metrohm Applikon B.V.) was conducted with an emphasis on examination of
10 accuracy and precision associated with processing of chromatograms. Using laboratory standards
11 and atmospheric measurements, analytical accuracy, precision, and method detection limits
12 derived using the commercial MARGA software were compared to an alternative
13 chromatography procedure consisting of a custom Java script to reformat raw MARGA
14 conductivity data and Chromeleon (Thermo Scientific Dionex) software for peak integration.
15 Our analysis revealed issues with accuracy and precision resulting from misidentification and
16 misintegration of chromatograph peaks by the MARGA automated software as well as a
17 systematic bias at low concentrations for anions. Reprocessing and calibration of raw MARGA
18 data using the alternative chromatography method lowered method detection limits and reduced
19 variability (precision) between parallel sampler boxes. Instrument performance was further
20 evaluated during a one-month intensive field campaign in the fall of 2014, including analysis of
21 diurnal patterns of gaseous and particulate water soluble species (NH₃, SO₂, HNO₃, NH₄⁺, SO₄²⁻
22 and NO₃⁻), gas-to-particle partitioning, and particle neutralization state. At ambient
23 concentrations below ~ 1 µg/m³, concentrations determined using the MARGA software are
24 biased +30% and +10% for NO₃⁻ and SO₄²⁻, respectively, compared to concentrations determined
25 using the alternative chromatography procedure. Differences between the two methods increase
26 at lower concentrations. We demonstrate that positively biased NO₃⁻ and SO₄²⁻ measurements
27 result in overestimation of aerosol acidity and introduce non-trivial errors to ion balances of
28 inorganic aerosol. Though the source of the bias is uncertain, it is not corrected by the MARGA
29 online single-point internal LiBr standard. Our results show that calibration and verification of
30 instrument accuracy by multi-level external standards is required to adequately control analytical
31 accuracy. During the field intensive, the MARGA was able to capture rapid compositional



32 changes in PM_{2.5} due to changes in meteorology and air mass history relative to known source
33 regions of PM precursors, including a fine NO₃⁻ aerosol event associated with intrusion of arctic
34 air into the southeast U.S.

35

36 1. Introduction

37

38 Secondary inorganic aerosols are formed from gaseous precursors including
39 ammonia (NH₃), nitric acid (HNO₃) and sulfur dioxide (SO₂), producing ammonium nitrate
40 (NH₄NO₃), ammonium bisulfate (NH₄HSO₄) and ammonium sulfate ((NH₄)₂SO₄) particles.
41 These gaseous precursors and particulate matter, which partition between phases to establish a
42 thermodynamic equilibrium of ammonium-sulfate-nitrate (Finlayson-Pitts and Pitts, 2000;
43 Seinfeld and Pandis, 2006), represent a significant fraction of PM_{2.5} (Seinfeld and Pandis, 2006;
44 Pinder et al., 2007) and contribute to atmospheric deposition of nutrients and acidity. The
45 implementation of National Ambient Air Quality Standards has reduced emissions of NO_x and
46 SO₂; however, NH₃ is not regulated and has not been routinely monitored until relatively
47 recently (Puchalski et al, 2015). Nevertheless, to further reduce fine particulate matter,
48 controlling NH₃ emissions has been suggested to be more cost-effective than further reductions
49 of NO_x and SO₂ in some cases, (Vayenas et al, 2005; Pinder et al., 2007). Reduction of NH₃
50 emissions may also represent the most effective strategy for reducing atmospheric nitrogen
51 deposition to acceptable levels (Li et al., 2016) in some ecosystems. High-frequency
52 simultaneous measurements of the gas and aerosol components of the ammonium-sulfate-nitrate
53 system are required to investigate inorganic aerosol characteristics (e.g., phase partitioning,
54 acidity) and formation processes and to quantify the dry component of nitrogen deposition.

55 Traditionally, integrated denuder and/or filter based techniques (i.e., 24 hours or longer)
56 have been used to monitor inorganic aerosols and their precursors (Trebs et al 2004 and
57 references therein; Benedict et al., 2013; Chen et al., 2014). The disadvantages of poor temporal
58 resolution and labor intensity as well as positive and negative sampling artifacts make these
59 methods difficult to deploy for extended periods of time and of limited use for characterization
60 of rapidly changing atmospheric conditions. Recent development of near real-time semi-
61 continuous analyzers, including the Particle-Into-Liquid sampler (PILS-IC, Metrohm AG,
62 Herisau, Switzerland), Particle-Collector-Ion Chromatograph (PC-IC), Aerosol Mass
63 Spectrometer (AMS, Aerodyne Research Inc., USA), Ambient Ion Monitor-Ion Chromatograph



64 (AIM-IC, URG Corp. And Dionex Inc., USA) and the Monitor for AeRosols and Gases
65 (MARGA, Metrohm Applikon B.V., the Netherlands) facilitate monitoring inorganic
66 atmospheric constituents with much higher time resolution (Jayne et al., 2000; Weber et al.,
67 2001; Al-Horr et al., 2003; Trebs et al., 2004; Schaap et al., 2011; Markovic et al., 2012). A
68 version of the MARGA incorporating two sample boxes (MARGA 2S), similar to the system
69 described here, has recently been used to quantify dry deposition using a micrometeorological
70 gradient flux method (Rumsey and Walker, 2016).

71 MARGA's capability of near real-time (hourly) simultaneous measurement of water
72 soluble particulate species as well as their gaseous precursors makes it a state-of-art research
73 instrument. Such time-resolved measurements allow investigation of highly time sensitive,
74 rapidly changing pollution episodes as well as aerosol processes such as gas/particle partitioning
75 and neutralization state. The MARGA has been deployed in widely varying environments to
76 monitor ambient gaseous and particulate water soluble species including NH_3 , SO_2 , HNO_3 ,
77 NH_4^+ , SO_4^{2-} and NO_3^- (Schaap et al., 2011; U.S. EPA, 2011; Makkonen et al., 2012; Mensah et
78 al., 2012; Khezri et al., 2013; Huang et al., 2013; Rumsey et al., 2014; Shi et al., 2014; Allen et
79 al., 2015; Twigg et al., 2015; Rumsey and Walker, 2016). Although the MARGA denuder and
80 steam jet aerosol collector (SJAC) have been evaluated for collection efficiency of gases and
81 particles (Wyers et al., 1993; Khlystov et al., 1995), there is relatively limited data on accuracy
82 and precision of concentration measurements (Weber et al., 2003; Trebs et al., 2004; Makkonen
83 et al., 2012; Lee et al., 2013; Phillips et al., 2013; Rumsey et al., 2014; Allen et al., 2015).
84 Phillips et al. (2013) found that HNO_3 determined by the MARGA's wet rotating denuder
85 displays a cross-sensitivity to N_2O_5 . The magnitude of the resulting positive bias in HNO_3 is
86 highly dependent on the ambient conditions (eg. NO_x , O_3 , biogenic VOC concentrations and
87 temperature) responsible for N_2O_5 production. Lee et al. (2013) observed differences SO_4^{2-} ,
88 NH_4^+ and NO_3^- at a suburban site in Hong Kong where an AMS instrument measured only 33-
89 60% of the PM mass measured by a collocated MARGA. Part of the difference was attributed to
90 different particle size cut of the inlets used ($\text{PM}_{1.0}$ for AMS and $\text{PM}_{2.5}$ for MARGA). Rumsey et
91 al. (2014) compared the MARGA to a reference time-integrated denuder/filter pack system. SO_2 ,
92 SO_4^{2-} and NH_4^+ agreed within 15% between the two systems; however, HNO_3 and NH_3
93 comparisons showed an underestimation by MARGA of 30%, mostly likely due to loss to the
94 surface of the long (≈ 4 m) polyethylene sample tubing used. Though differences between the



95 MARGA and other measurement systems have been observed, the extent to which the
96 differences may be attributable solely to chromatography has not been evaluated.

97 The objective of this study is to evaluate MARGA performance with a focus on accuracy
98 and precision characteristics related to automated chromatography analysis. Specifically, we
99 investigate misidentification and misintegration by the MARGA software as well as errors and
100 uncertainties resulting from such issues. To aid efficiency and flexibility in the reprocessing of
101 MARGA chromatograms, an alternative chromatography procedure, based on offline analysis of
102 raw MARGA data, was employed. Using laboratory standards, analytical accuracy, precision,
103 and method detection limits derived from the two chromatograph processing methods were
104 compared. Field measurements were used to further evaluate instrument performance and to
105 demonstrate the ability of the MARGA instrument to resolve important atmospheric processes,
106 including diurnal patterns of observed gaseous (NH_3 , SO_2 , HNO_3) and particulate water soluble
107 species (NH_4^+ , SO_4^{2-} and NO_3^-), fine particle neutralization state, and changes in atmospheric
108 composition related to synoptic meteorological patterns. Using aerosol neutralization state as a
109 case study, the impact of chromatography errors on measurement accuracy was assessed.

110

111 2. Methods and materials

112 2.1 MARGA system

113 Details and principles of the MARGA system have been previously described (Rumsey et
114 al., 2014; Rumsey and Walker, 2016). Briefly, the MARGA sampler box consists of a wet
115 rotating denuder (WRD) and a steam jet aerosol collector (SJAC), which enables semi-
116 continuous collection and measurement of gaseous and water soluble inorganic particulate
117 species in the ambient air. When drawn through the WRD, gaseous species are collected by
118 diffusion into a liquid film while particles pass through the WRD to the SJAC where super-
119 saturation grows the particles by condensation. Liquid samples from the WRD and SJAC are
120 continuously collected in individual syringes and analyzed by Ion Chromatography (IC) on an
121 hourly basis at the detector unit. By employing two sets of liquid syringes, a set of samples is
122 collected while samples from the previous hour are analyzed. To monitor accuracy and
123 automatically adjust concentrations, liquid samples are mixed with an internal lithium bromide
124 (LiBr) standard at a fixed ratio before injection for IC analysis.

125

126 2.2 Chemical materials



127 DI water (18.2 MΩ·cm, Milli-Q Reference system, Millipore) with 10 ppm H₂O₂ (30%
128 certified ACS grade, Fisher Scientific) was used as absorbance solution for the MARGA WRD
129 and SJAC sample collection. H₂O₂ was added to prevent bacteria growth and subsequent loss of
130 NH₄⁺. The MARGA internal standard LiBr (>99%, ACROS Organics) aqueous solution was
131 prepared at concentrations of 320 μg/L Li⁺ and 3680 μg/L Br⁻. Solid chemical standards
132 NH₄NO₃, NH₄Cl, (NH₄)₂SO₄, NaNO₃, KCl, CaCl₂ · 2H₂O and MgSO₄ · 7H₂O (≥99% certified
133 ACS grade, Fisher Scientific) were used to prepare stocks and various levels of liquid external
134 standards. Certified aqueous analytical standard solutions purchased from Alltech Associates
135 (Anion Mix 1, Cation Mix B, Alltech Associates, Inc) served as accuracy check standards. We
136 note here that “internal” standard refers to the MARGA LiBr standard that is mixed with every
137 MARGA liquid sample immediately upstream of the IC injection loop. “External” standards
138 refer to liquid standards that are introduced at the WRD and SJAC, as described in more detail
139 below.

140

141 2.3 Chromatography

142 MARGA proprietary chromatography software consists of an online version used for
143 automated analysis when the instrument is in measurement mode and a “MARGA tool”, so
144 named by the manufacturer, used for offline analysis of chromatograms, either individually or in
145 batches, but otherwise identical to the online version. In both cases, liquid analyte concentrations
146 are determined by calculating the total amount of injected sample directly from the conductivity
147 measurement following the method of van Os et al. (1984). As mentioned previously, accuracy
148 is controlled by adjusting the measured concentration based on a single point internal LiBr
149 standard, at a working concentration of 320 μg/L of Li⁺ and 3680 μg/L of Br⁻, which is injected
150 with each sample. The MARGA software does not employ a multipoint calibration curve.

151 During post processing of field data, it was discovered that peaks integrated by the
152 MARGA tool showed a certain degree of misidentification and inconsistent integration. Specific
153 integration issues include incorrectly defined baseline due to peak fronting and tailing and
154 shifting between “drop perpendicular” and “valley to valley” integration options among samples
155 (shown in Supplemental Information). As indicated by the examples shown in Supplemental
156 Information, baseline selection by the MARGA tool could vary from sample run to run, which
157 could introduce significant errors and uncertainties. Integration issues are particularly



158 problematic when the IC analytical columns deteriorate due to extended use. Under such
159 conditions, unresolved peaks occurred more frequently.

160 In addition to misidentification and misintegration issues with the MARGA software,
161 reintegration of individual peaks with the MARGA tool was found to be inefficient and
162 inflexible. Although the MARGA tool contains adjustable integration parameter settings such as
163 peak search sensitivity and peak search smoothing, the parameters are applied to all
164 chromatograms. For example, the adjusted parameter may achieve the desired integration for a
165 particular misintegrated peak, but other peaks which were deemed as integrated properly prior to
166 any adjustments may subsequently be improperly integrated. The inability to manually adjust
167 the integration for individual peaks makes post-processing of chromatograms time consuming.
168 Hence, an alternative chromatography software (Chromeleon V7.2, Thermo Scientific Dionex)
169 was tested for reprocessing of MARGA chromatograms.

170 In order to import MARGA generated chromatograms to the Chromeleon
171 chromatography data processing system, raw MARGA chromatography data (.dat format) were
172 converted to time series of conductivity (.txt format) using the MARGA tool. Using the
173 Chromeleon generated template (.cdf format) file, as well as a custom Java script, a batch of
174 MARGA conductivity time series (.txt format) files are converted to their corresponding .cdf
175 format. A folder of conductivity data files in cdf format is then imported to Chromeleon for
176 chromatogram reprocessing.

177 MARGA and Chromeleon approaches were compared in terms of peak areas and
178 calculated concentrations of internal and external liquid standards, as well as determinations of
179 laboratory blanks, method detection limits, and air concentrations during ambient sampling. To
180 compare integration characteristics between the MARGA tool and Chromeleon software, a series
181 of external liquid standards (Table S1), representing a range of concentrations equivalent to \approx
182 $0.05 - 10.5 \mu\text{g}/\text{m}^3$ NH_4^+ , NO_3^- and SO_4^{2-} in air, were run through the MARGA instrument with
183 the air pumps and SJAC steam generator disconnected. This configuration allowed liquid
184 standards to pass through the entire sampling (i.e., WRD and SJAC and liquid sampling lines)
185 and analytical (i.e., syringes and ICs) components of the system. The resulting chromatograms
186 were used to generate a calibration curve using Chromeleon, in which peak areas were related to
187 liquid standard concentration ($\mu\text{g}/\text{L}$). These peak areas and concentrations were then compared
188 directly to peak areas and concentrations generated by the MARGA software (without any



189 further manual peak integration adjustment), the latter being adjusted only by the internal LiBr
190 standard. A certified accuracy check standard was used to evaluate the accuracy of the
191 calibration curves generated by Chromeleon and all of the analytes were found to be within the
192 10% accuracy check criteria. System blanks using absorbance solution were evaluated in the
193 same manner as the external liquid standards. Finally, both the MARGA internal standard (LiBr)
194 and a subset of the external standards were verified by independent analysis on a Dionex ICS-
195 2100 (Thermo Scientific, Waltham, MA) multi-point calibrated with additional certified
196 standards. Due to different loop size and corresponding detection limit of the Dionex system,
197 only a subset of the external standards was independently verified.

198

199 2.4. Field study

200 Field measurements were conducted in a grass field at the Blackwood Division of Duke
201 Forest (35.98°N, 79.09°W) near Chapel Hill, NC. Duplicate MARGA sample boxes (SB1 and
202 SB2) were positioned in parallel (i.e., collocated) with inlets \approx 1.5 m above the ground. Both
203 MARGA sample boxes employed a Teflon coated cyclone-type inlet with an aerodynamic 2.5
204 μ m cut size at a flow rate of 16.7 LPM (URG-2000-30EH, University Research Glassware
205 Corporation). A short (0.2 m) length of 25.4 mm O.D. Teflon tubing connected the atmospheric
206 inlet to the MARGA denuder. MARGA sampler and detector boxes were equipped with weather
207 protection enclosures which were temperature controlled at 25°C.

208 Sampler air flow rates were measured and verified weekly by connecting a NIST
209 traceable primary standard flow meter (Bios DryCal DC-Lite flowmeter, Mesa Laboratories,
210 Inc., Lakewood, CO) to the sampler inlets. Based on the calibration by the flow meter, MARGA
211 reported flow rates were overestimated by 6% and 8% for sample box 1 (SB1) and 2 (SB2),
212 respectively, and air concentrations were adjusted accordingly. Initial data validation was
213 conducted by monitoring the MARGA automated status codes; data with internal standard LiBr
214 responses outside of \pm 10% nominal concentrations were invalidated and excluded from further
215 analysis.

216 To compare air concentrations derived from MARGA and Chromeleon software, the
217 liquid calibration curves (see above section 2.2) generated by Chromeleon were used to calculate
218 liquid concentrations, and by combining with air and liquid flow rates, corresponding air
219 concentrations were derived. The Chromeleon derived air concentrations were then compared to



220 air concentrations generated by the MARGA software, which used only the internal LiBr
221 standard as a calibration adjustment. For this comparison, the same air and liquid flow rates were
222 used. Both sets of air concentrations were corrected for system blanks and air flow rate
223 calibrations. The MARGA was operated continuously in the field from 15 October to 17
224 November 2014. However, due to a failure of the IC degasser unit, no valid data were generated
225 from 31 October to 2 November 2014.

226

227 2.5. Ancillary field data

228 A 10 m meteorological station is maintained and managed at Duke Forest by the North
229 Carolina Division of Forest Resources and Bureau of Land management. Verified hourly
230 metrological data were obtained online: (<http://mesowest.utah.edu>). Concentrations of PM_{2.5}
231 mass (TEOM model 1400ab, R&P Thermo Scientific, Franklin, MA) and organic/elemental
232 carbon (OC/EC, Model 4 Semi-continuous field analyzer, Sunset Laboratory, Inc., Hillsborough,
233 NC) were measured adjacent to the MARGA instrument. Backward air mass trajectories were
234 calculated for select periods using the Hybrid Single Particle Lagrangian Integrated Trajectory
235 (HYSPPLIT) model (Draxler and Rolph, 2003) with NOAA ARL EDAS 40 km meteorological
236 data. Trajectories were run for 168 hour periods at an arriving height of 500 m above the ground
237 level. To aid interpretation of the back trajectories, facility emission inventory data for NO_x, SO₂,
238 and NH₃ were retrieved from the 2011 National Emission Inventory database
239 (<http://www.epa.gov/ttn/chief/net/2011inventory.html>).

240

241 3 Results and discussion

242 3.1. Laboratory study of chromatography characteristics

243 MARGA chromatograms were systematically examined by running a series of liquid
244 external standards over a range of concentrations listed in Table S1. Each standard level was
245 analyzed for approximately 20 hours, producing $N = 80$ observations for 4 analytical channels
246 combined (two sample boxes for gas and aerosol channels). The same sets of chromatograms
247 were re-processed by Chromeleon to generate multi-point calibration curves for each analyte.
248 Peaks that were obviously misintegrated by the MARGA tool were not included in this analysis.
249 Relationships between peak area and standard concentration were linear except for SO₄²⁻, for
250 which a polynomial fit was adopted to better represent the entire concentration range. All



251 calibration curves had r^2 values > 0.999 . A certified check standard was used to evaluate the
252 accuracy of the calibration curves generated by Chromeleon and all analytes were found to be
253 within the 10% accuracy check criteria. Using absorbance solution to assess contamination,
254 blank concentrations of NO_3^- and SO_4^{2-} reported by Chromeleon were 0.002 and $0.080\mu\text{g}/\text{m}^3$,
255 respectively, while the corresponding system blanks determined by the MARGA tool were 0.018
256 and $0.109\mu\text{g}/\text{m}^3$. NH_4^+ was not detectable in the blank solution.

257 Table 1 lists estimated method detection limits for the species of interest calculated using
258 both the MARGA tool and Chromeleon. Method detection limits were calculated as
259 $2.58 \times$ standard deviation of the lowest detectable external standards, a statistical method
260 described in detail by Currie (1999). Method detection limits calculated using the MARGA
261 software are substantially larger than corresponding detection limits calculated with Chromeleon,
262 indicating more variability in the MARGA integrations from sample to sample. Such
263 inconsistency will translate to larger uncertainties for low concentration samples. This is
264 particularly important when attempting to resolve very small differences between two MARGA
265 sample boxes, a requirement for flux gradient applications (Rumsey and Walker, 2016). Error
266 propagations inherited from misintegration could be minimized by reexamining the
267 chromatograms. We note that the detection limits of the instrument evaluated here are larger,
268 particularly for anions, than those reported by Rumsey and Walker (2016), which used the same
269 MARGA software but a different instrument. This indication of variability demonstrates the
270 need to characterize individual measurement systems. The detection limits calculated with
271 Chromeleon are more similar to those reported by Rumsey and Walker (2016).

272 Table S2 lists the internal standard peak areas as integrated by the MARGA tool and
273 Chromeleon for each of the corresponding external standard levels. Note that while the
274 concentrations of anions and cations in the external standards vary by level, the actual
275 concentration of the internal standard does not. For both Li^+ and Br^- , systematically larger peak
276 areas are calculated by the MARGA software. While the systematic difference for Br^- is rather
277 consistent (17%), differences in Li^+ between the two software techniques decrease with
278 increasing external standard concentration. As the peak areas of Na^+ and NH_4^+ increase, the close
279 retention times of Na^+ , NH_4^+ , and Li^+ cause the peaks to appear more like unresolved lumps (i.e.,
280 peak merging effect). At these higher standard concentrations, the MARGA software
281 underestimated the Li^+ peak area relative to Chromeleon and integration became less consistent



282 from sample to sample. This is likely due to the MARGA software frequently shifting between
283 “drop perpendicular” and “valley to valley” integration options between samples, introducing
284 more variability to the calculated areas (see Supplemental Information Figure S1). For
285 consistency, the “drop perpendicular” integration option was adopted for all Chromeleon
286 reprocessing. We observed that as the concentration levels increase, the errors due to adopting
287 different integration options could be as much as 6% at the highest external standard
288 concentration equivalent to $\approx 10.5 \mu\text{g}/\text{m}^3$. In summary, the consistent 17% difference in Br^- peak
289 areas between software packages is not necessarily a source of error in the final calculation of
290 MARGA liquid concentrations. For Li^+ , the variability in integration and decrease in the
291 difference in peak area between the two software packages at higher standard levels would
292 translate to systematic differences in corresponding NH_4^+ liquid concentrations above ≈ 100
293 $\mu\text{g}/\text{L}$ ($\approx 2.5 \mu\text{g}/\text{m}^3$ in air).

294 In addition to underestimation of Li^+ , other issues associated with MARGA processing of
295 cation chromatograms include misidentification of NH_4^+ as Na^+ when a negligible Na^+ peak
296 existed and misidentification of NH_4^+ and Na^+ peaks together as a single NH_4^+ peak. For anion
297 chromatograms, NO_3^- peaks were rather frequently discovered as not identified at all; SO_4^{2-}
298 peaks were found to have an incorrectly defined baseline due to peak fronting and tailing (see
299 Supplemental Information Figures S2 - S5). These issues become more prevalent with column
300 age.

301

302 3.2 Field study

303 In order to assess the potential impact of chromatography related analytical errors
304 observed during the laboratory evaluation, MARGA performance was further investigated during
305 a one-month field campaign. Air concentrations generated by the MARGA tool and Chromeleon
306 are compared over a range of chemical and meteorological conditions, using particle
307 neutralization state as a case study. Intrusion of arctic air into the southeast U.S. provided an
308 opportunity to observe rapidly changing and distinct patterns of gas-to-particle partitioning
309 within the ammonium-nitrate-sulfate system. In the following sections, air concentrations
310 presented in time series and summary statistics describing ambient measurements were generated
311 by Chromeleon unless otherwise indicated.

312



313 3.2.1 MARGA accuracy

314 Chromatograms reprocessed by the MARGA tool were individually examined and
315 concentrations were filtered for periods of instrument malfunction, peak misintegration, and LiBr
316 internal standard outside $\pm 10\%$ of the nominal target concentration. This filtering procedure
317 would include low concentrations in which there was an obvious problem with the original peak
318 integration. Filtered data were not included in the comparison between the MARGA tool and
319 Chromeleon. Table S3 presents the percentage of data excluded from the comparison. NO_3^-
320 peaks appeared to be the analyte most affected, especially in the case of HNO_3 (up to 6.2% of the
321 data). At sampling sites where HNO_3 concentrations are typically below $1\mu\text{g}/\text{m}^3$, data rejection
322 may be more extensive.

323 Air concentrations derived from the MARGA and Chromeleon software approaches were
324 compared by ordinary least squares regression using Chromeleon as the reference (Figure 1).
325 Over the entire range of conditions, concentrations calculated using the MARGA tool were
326 within 5% (slopes, Figure 1), on average, of those reported by Chromeleon for SO_4^{2-} , SO_2 , NH_4^+
327 and NH_3 . Very good agreement is observed for NH_4^+ and NH_3 , with slopes close to unity and
328 intercepts near zero. As concentrations were below $2.5\mu\text{g}/\text{m}^3$, potential disagreement resulting
329 from differences in cation integration at higher concentrations (section 3.1) was not observed.
330 Although the accuracy of NO_3^- was poorer, it was within 10%, overall. By contrast, HNO_3
331 concentrations, which were mostly below $1.0\mu\text{g}/\text{m}^3$, showed a positive bias of approximately
332 30%. Correlation of HNO_3 between the MARGA tool and Chromeleon also revealed a more
333 scattered pattern compared to other analytes. The 30% positive bias in MARGA HNO_3 results is
334 also observed for NO_3^- concentrations below $\approx 1.0\mu\text{g}/\text{m}^3$ (Supplemental Information Figure S6).
335 Restricting the NO_3^- regression comparison to lower concentrations results in slopes of ≈ 1.4 and
336 1.5 over concentration ranges of $0 - 0.5\mu\text{g}/\text{m}^3$ and $0 - 0.25\mu\text{g}/\text{m}^3$, respectively, with intercepts
337 near zero; the disagreement increases at concentrations below $0.25\mu\text{g}/\text{m}^3$. SO_2 and SO_4^{2-} results
338 also show positive bias in the MARGA results at lower concentrations, though not as large as
339 observed for HNO_3 and NO_3^- . For SO_2 , slopes of ≈ 1.1 , 1.15, and 1.2 are observed over
340 concentration ranges of $0 - 1.0\mu\text{g}/\text{m}^3$, $0 - 0.5\mu\text{g}/\text{m}^3$, and $0 - 0.25\mu\text{g}/\text{m}^3$, respectively, with
341 intercepts near zero. Agreement improves at concentrations above $1.0\mu\text{g}/\text{m}^3$ as the slope
342 approaches unity. Over the entire range of conditions, SO_4^{2-} also shows good agreement, on
343 average, though with a significant offset ($0.14\mu\text{g}/\text{m}^3$, Figure 1). At lower concentrations



344 (Supplemental Information Figure S6), a pattern of disagreement similar to SO₂ emerges; over
345 the range 0 – 1.0 µg/m³, a slope and intercept of 1.09 and 0.09 are observed, respectively.
346 Similar discrepancy patterns were observed for SO₄²⁻ and NO₃⁻ when lower level external
347 standards were tested. In contrast to anions, cation results showed consistently good agreement
348 even at low concentrations.

349 The source of bias between the MARGA and Chromeleon results may result from several
350 factors: 1) MARGA overestimation from incorrectly defined peak start and end points due to
351 peak fronting and tailing; 2) incorrect baseline definition for smaller peaks (i.e., low observed
352 HNO₃ and NO₃⁻ concentrations) as compared to larger peaks; or perhaps the most likely
353 explanation, 3) inability of the van Os method used by the MARGA software to fully linearize
354 the relationship between peak area and liquid concentration at low concentrations. As noted
355 above, the method of van Os et al. (1984) for anion analysis with chemical suppression allows
356 calculation of the sample concentration directly from the conductivity measurement. van Os et
357 al. concluded that relationships between the amount of sample injected and total peak area were
358 linear over the range 2.0 – 40.0 mg/L. It was noted, however, that calculated concentrations at
359 the 1.0 mg/L standard level, the lowest concentration tested, were slightly low for NO₃⁻ and Cl⁻
360 and slightly high for SO₄²⁻. Subsequently, the 1.0 mg/L standard level was not used in the final
361 regression analysis used to test the linearity of the method. Accounting for differences in
362 injection loop size between studies, the 1.0 mg/L level used by van Os et al. (1984) is a factor of
363 2 to 2.5 larger than the highest standard concentration tested in our study (Table S1) and a factor
364 of 25 (SO₂) to 125 (HNO₃) larger than the corresponding average observed air concentrations
365 (Table 2). It is possible that the method of van Os et al. (1984) systematically over-predicts
366 anion concentrations at the lower concentrations observed in our study. This accuracy issue
367 would not be controlled by the single point Br⁻ internal standard (3680 µg/L), which is within the
368 linear response range of anion concentrations tested by van Os et al. (1984).

369 The NO₃⁻ bias observed here may help to explain the results of previous studies. Five
370 semi-continuous analyzers, which included an earlier version of a Wet-Annular Denuder/Steam-
371 Jet Aerosol Collector (Trebs et al., 2004, 2008) that predates the commercialized MARGA, were
372 evaluated and inter-compared by Weber et al. (2003) for measurements of NO₃⁻ and SO₄²⁻ in
373 PM_{2.5} at the Atlanta EPA supersite. The earlier version MARGA analyzer showed a range of
374 25% to 34% significantly higher NO₃⁻ concentration as compared to a group mean of the five



375 semi-continuous monitors evaluated while measured SO_4^{2-} agreed well (within 10%). This
376 discrepancy was suspected to be a sampling artifact of NO_3^- formed from NO_x in the MARGA
377 particle steam collector, though there was a lack of correlation with measured NO_x . Four
378 instruments including a MARGA, an AMS, a denuder difference analyzer as well as an
379 integrated nylon filter based IMPROVE sampler were evaluated by Allen et al. (2015) during the
380 2013 Southern Oxidant and Aerosol Study (SOAS) campaign for particulate NO_3^- . The
381 MARGA measured much higher NO_3^- concentrations than the other three analyzers at this
382 southeastern US site where NO_3^- was mostly below $1.0 \mu\text{g}/\text{m}^3$ during the sampling period.
383 Differences in inlet cyclone size cuts and cyclone efficiencies for supermicron particles may be
384 partly responsible. However, these examples of significantly higher MARGA NO_3^- relative to
385 other methods, as well as the results of this study, warrant further investigation of potential
386 chromatography related biases.

387

388 3.2.2 MARGA precision

389 Precision statistics (Table 2) were derived from orthogonal least squares regression (Wolff
390 et al., 2010) of concentrations from the two MARGA sample boxes operated in parallel (i.e.,
391 collocated). Orthogonal least squares acknowledges uncertainty in both the X and Y variables
392 (i.e. measurements from both sample boxes) and the standard deviation of the residuals of the
393 regression is therefore a measure of the overall precision of the MARGA system. Concentrations
394 of particulate NO_3^- , SO_4^{2-} , NH_4^+ , gaseous SO_2 and NH_3 agree well between the sample boxes,
395 with slopes within 5% of unity and negligible intercepts (Table 2), indicating no significant
396 systematic differences between the two sample boxes. The standard deviations (precision) and
397 relative standard deviations (RSD, expressed as a percentage of the average air concentrations)
398 of the regression residuals reported here ($\mu\text{g}/\text{m}^3$) for NO_3^- , SO_4^{2-} , NH_4^+ , and NH_3 are similar (<
399 10% RSD) to those reported by Rumsey and Walker (2016). The lower precision for SO_2
400 reported here is most likely related to larger differences in concentration between sample boxes
401 during periods of rapid concentration changes associated with the arctic air episode (Figures 2
402 and 3).

403 Relative to the other analytes, HNO_3 showed a much more significant difference between
404 the two sampler boxes (regression slope of 0.83). Additionally, HNO_3 precision (15.8% RSD)
405 was much lower than observed for NO_3^- aerosol (4.8% RSD) at nearly identical average



406 concentrations. These findings, in combination with the excellent agreement between sample
407 boxes for NO_3^- , suggest that the HNO_3 measurements were influenced by inlet, rather than
408 analytical, issues. As indicated by the much higher Henry's law coefficient of HNO_3 relative to
409 NH_3 and SO_2 , HNO_3 is "sticky" and therefore more prone to inlet losses as well as re-evaporation
410 from inlet/tubing surfaces. Although the inlet cyclones used were Teflon coated, and the Teflon
411 tubing connecting the cyclone to the WRD was very short (0.2 m), our results suggest
412 differences in transmission efficiencies of the two inlets. Similar difficulties in sampling HNO_3
413 have been reported previously for studies in which size selective inlets and/or significant lengths
414 of sample tubing were used for MARGA sampling (Trebs et al., 2004; Rumsey et al., 2014;
415 Allen et al., 2015). In our study, the length of inlet tubing between the cyclone and WRD was
416 similar to the length of tubing (0.3 m) used by Rumsey and Walker (2016), the difference being
417 that no size selective inlet was used by Rumsey and Walker. In their study, multiple collocation
418 experiments showed much better agreement, on average, between the two sample boxes and
419 better precision (5.8% RSD), suggesting that the cyclone may be the primary source of
420 disagreement between sample boxes in the current study. It is important to note, however, that
421 concentrations of HNO_3 observed in the current study were generally very low, averaging 0.19
422 $\mu\text{g}/\text{m}^3$ over the study period. Such low concentrations contribute to greater relative variability
423 between sample boxes. Our results re-emphasize the requirement of low affinity tubing and inlets
424 with respect to both materials and surfaces/lengths for HNO_3 sampling.

425

426 3.2.3 Temporal patterns of gas and particle concentrations

427 Figure 2 shows time series of hourly gas phase concentrations of HNO_3 , SO_2 and NH_3 ,
428 and particle phase NO_3^- , SO_4^{2-} and NH_4^+ (as local time (EDT)). From mid-October to mid-
429 November, meteorological conditions were mild and humid (Figure 3), which is typical of fall in
430 the southeast U.S. However, an arctic outbreak of cold air impacted the site from 13 to 17
431 November, accompanied by much lower temperature and relative humidity. Wind speed was
432 typical of the site, averaging 2 m/s. The prevailing wind directions were northwest and southwest
433 before the cold air period and northerly during the dry and cold period.

434 Figure 4 shows the diurnal pattern of gas and particle concentrations. Only days with
435 hourly data coverage greater than 65% were used for calculating diurnal profiles ($N = 26$). NH_4^+
436 and SO_4^{2-} exhibited a single mode pattern with a peak around 9-11 am local time. NO_3^- showed a



437 similar peak in the morning and a smaller peak at 9-11 pm. Morning peaks most likely represent
438 the downward mixing of aerosols from aloft when the nocturnal boundary layer breaks down.
439 The second peak of NO_3^- at night may be related to night time NO_3^- radical chemistry
440 (Finlayson-Pitts and Pitts, 2000; Seinfeld and Pandis, 2006) leading to formation of particulate
441 NO_3^- . The mid-afternoon (2-3pm) peak in gas phase HNO_3 results from photochemical
442 processing of NO_x . NH_3 showed a much broader afternoon peak, which may reflect local
443 emissions from natural sources during warmer afternoon periods. The diurnal pattern of SO_2
444 showed a pronounced peak around 10-11 am, and two less pronounced peaks at 8 pm and 1 am,
445 respectively. This pattern may reflect the competition between emission and dry deposition, as
446 well as boundary layer dynamics: higher emissions during the day versus slower dry deposition
447 rates and shallower boundary layer at night. The diurnal pattern is also affected by the large SO_2
448 spikes observed during the arctic air mass period, presumably associated with increased
449 emissions resulting from greater energy demand.

450 Gas/particle partitioning presented as fraction in the particle phase is shown in Figure 5.
451 In order to examine the aerosol neutralization state, chemical composition ratios were calculated
452 as:

$$453 \quad R1 = \frac{\text{NH}_4^+}{\text{SO}_4^{2-}} \quad (1)$$

454

$$455 \quad R2 = \frac{\text{NH}_4^+}{\text{NO}_3^- + 2 \times \text{SO}_4^{2-}} \quad (2)$$

456

457 where ratios R1 and R2 are molar concentration based. $R1 = 2$ reflects an aerosol entirely
458 composed of $(\text{NH}_4)_2\text{SO}_4$, which is the fully neutralized state of SO_4^{2-} . $R1 > 2$ indicates the
459 presence of NH_4NO_3 in addition to $(\text{NH}_4)_2\text{SO}_4$, while $R1 < 2$ signifies a state of NH_4^+ deficit
460 indicative of an acidic aerosol. Moreover, a ratio of $R2 = 1$ indicates a fully neutralized aerosol
461 containing NH_4NO_3 and $(\text{NH}_4)_2\text{SO}_4$, while $R2 > 1$ represents as condition of excess NH_4^+ . A
462 value of $R2 < 1$ suggests acidic aerosol comprising NH_4NO_3 and a combination of NH_4HSO_4 and
463 $(\text{NH}_4)_2\text{SO}_4$ or, alternatively, NO_3^- associated with supermicron particles from aged sea salt or
464 crustal materials (Allen et al., 2015).

465 Two distinct periods of contrasting aerosol composition were observed (Figure 5d). With
466 $R1$ mostly less than 2 and $R2$ less than or close to 1, aerosol measured during October primarily



467 comprised NH_4HSO_4 and $(\text{NH}_4)_2\text{SO}_4$. When R1 approached 1 for three short episodes in October,
468 particles most likely existed solely as NH_4HSO_4 . The observed acidity most likely suppressed
469 NO_3^- partitioning and formation, which is reflected by a significant decrease in the molar ratio of
470 NO_3^- in aerosol phase to as low as 0.1-0.2 (Figure 5a). Limited aerosol NO_3^- formation was also
471 reported by Allen et al. (2015) at a southeastern US (SOAS) site where aerosol was acidic. By
472 contrast, R1 was mostly above 2 in November, indicating the presence of NO_3^- . From 13 to 17
473 November, R1 reached as high as 4. Nevertheless, R2 was generally close to 1 during November,
474 indicating an aerosol comprised of NH_4NO_3 and $(\text{NH}_4)_2\text{SO}_4$. In contrast to the SO_4^{2-} dominated
475 October period, NO_3^- was a much greater contributor to inorganic aerosol in November; molar
476 concentrations of NH_4NO_3 even surpassed $(\text{NH}_4)_2\text{SO}_4$ when R1 reached 4 during the cold air
477 event. It should be noted that only acidity from inorganic species was examined in this study and
478 the ion balance could be further affected if organic acids were present and taken into account.

479 As noted above and illustrated in Figure S6, a positive bias in NO_3^- and SO_4^{2-} resulting
480 from peak integration and processing with the MARGA tool is observed for air concentrations
481 below $\sim 1.0 \mu\text{g}/\text{m}^3$. Our field study provides an opportunity to quantify the impact of these errors
482 over a range of chemical and meteorological conditions. For this analysis, the difference
483 between hourly concentrations determined by the MARGA versus Chromeleon software was
484 calculated as a percent relative to the Chromeleon result (i.e., $100\% \cdot (\text{MARGA} -$
485 $\text{Chromeleon})/\text{Chromeleon}$). Overall statistics of the hourly relative differences are summarized
486 in Figure 5e, including differences in phase partitioning (i.e., molar ratios calculated as
487 $\text{particle}/(\text{particle} + \text{gas})$) and neutralization state (R1 and R2). As expected, differences in the
488 $\text{NH}_4^+/\text{NH}_3$ partitioning ratio are near zero because no bias was observed between Chromeleon
489 and MARGA derived concentrations of NH_3 and NH_4^+ . Average and median differences in the
490 $\text{SO}_4^{2-}/\text{SO}_2$ partitioning ratio were similarly small, which is expected given that average SO_4^{2-}
491 and SO_2 concentrations were 1.41 and $0.98 \mu\text{g}/\text{m}^3$, respectively (Table 2). These concentrations
492 are above the level at which biases between MARGA and Chromeleon become significant. Mean
493 and median differences in the $\text{NO}_3^-/\text{HNO}_3$ partitioning ratio were $\approx -10\%$ and -1.5% ,
494 respectively, indicating a smaller ratio calculated with the MARGA software. As shown in
495 Figure 5e, the $\text{NO}_3^-/\text{HNO}_3$ partitioning ratio exhibits much larger hourly variability relative to
496 the other analytes, reflecting a combination of larger concentration bias and random error
497 associated with integration of very small peaks. The average relative difference in R1 was $\approx -$



498 13%, resulting from the combination of a constant offset and concentration dependent difference
499 between MARGA versus Chromeleon SO_4^{2-} results (section 3.2.1). Differences in R1 increase
500 non-linearly with decreasing SO_4^{2-} concentration, reaching $\approx -25\%$ at $0.5 \mu\text{g SO}_4^{2-} / \text{m}^3$. The
501 average relative difference in R2 was $\approx -14\%$, also exhibiting larger differences at lower
502 concentrations. Following the propagation of error in R2, differences are primarily driven by
503 much higher absolute concentrations of SO_4^{2-} relative to NO_3^- . Though absolute differences are
504 larger for NO_3^- concentrations, low concentrations result in a lesser contribution to the overall
505 difference in R2 between the MARGA and Chromeleon methods.

506

507 3.2.4 Arctic event

508 As noted above, an arctic outbreak of cold air impacted the site from 13 to 17 November.
509 The average temperature dropped from 12.9°C to 4.5°C during this period, with a minimum of -
510 3.9°C , which is well below normal for this site. RH ranged from 21 to 77% during the cold air
511 event. Total concentrations of gases plus particles were $\approx 2\text{X}$ higher during the cold arctic event
512 for NH_3 and NH_4^+ , SO_4^{2-} and SO_2 ; while for NO_3^- and HNO_3 , a factor of 5 difference was
513 observed (summary shown in Table 3). Though air was drier during the arctic event,
514 temperatures were cold enough to drive partitioning of gas phase inorganic compounds towards
515 the particle phase. In addition to elevated NO_3^- concentrations, three distinct episodes of SO_2
516 occurred, with a maximum concentration of $32.56 \mu\text{g}/\text{m}^3$ (Figure 2). Back trajectory analysis
517 (see Supplemental Information Figure S7) suggests that these SO_2 events reflect transport of
518 emissions from power plants and other point sources in the mid-west (see facility SO_2 emission
519 inventories Figure S8 in Supplemental Information). SO_2 from more local sources during the
520 extremely dry and cold arctic air conditions might also have contributed to the observed SO_2
521 spikes.

522 Gas and particle chemistry during the 13 to 17 November period, including TEOM $\text{PM}_{2.5}$
523 mass and elemental/organic (EC/OC) carbon concentrations, are examined in more detail in
524 Figure 6. This four-day period represents the highest concentrations of SO_4^{2-} , NH_4^+ , NO_3^- and OC
525 concentrations, as well as lowest temperature, observed during the study. However, total $\text{PM}_{2.5}$
526 mass showed less variability than the other species. Summaries of concentrations of gaseous and
527 particulate species are presented in Table 3 during and outside of the cold air event. In order to
528 better examine the arctic air mass intrusion, three sub-periods were selected, featuring a high



529 SO₄²⁻ episode; high NH₄⁺ and NO₃⁻ episode; and a high OC episode (individual periods are
530 marked and color coded in Figure 6). Inorganic components in particles demonstrated a pattern
531 of high concentrations for periods 1 and 2, while less so during period 3. Particulate organic
532 composition as represented by OC showed an opposite pattern, peaking in period 3. Differences
533 in time resolved concentrations of inorganic and organic species illustrate different emission
534 sources for inorganic and organic particulate pollutants. Back trajectories associated with the
535 three episodes are presented in Figure 6. For inorganic episodes 1 and 2, air masses originated
536 from the arctic and passed through the U.S. mid-west and Ohio River valley where emissions of
537 inorganic aerosol precursors, SO₂ and NO_x, from power plants and heavy industries were
538 encountered. Gas phase NH₃ concentrations are very low during these episodes, with the
539 majority of NH_x in the particle phase. By contrast, trajectories associated with the high OC
540 episode (period 3) suggest more of a northeastern origin and perhaps a greater influence of
541 residential wood burning associated with cold temperatures. During periods 1 and 2, inorganic
542 compounds contributed the majority of PM_{2.5} mass. The estimated sum of inorganics including
543 SO₄²⁻, NO₃⁻ and NH₄⁺ accounted for 61±31% and 83±24%, respectively of the PM_{2.5} mass for
544 period 1 and 2. In contrast, inorganic compounds only accounted for 22±11% of PM_{2.5} mass
545 during period 3.

546

547 4 Summary and conclusions

548 The MARGA is a state-of-art instrument that measures near real-time water soluble
549 particulate species as well as their gaseous precursors. The current commercial version of the
550 MARGA incorporates a continuous internal standard (LiBr) to verify and calibrate instrument
551 response for automated data generation and reporting. Close examination of MARGA
552 chromatograms revealed a number of issues, including misidentification and misintegration of
553 analyte peaks. Peak integration across similar chromatograms was found to be inconsistent with
554 the MARGA software shifting between integration options “drop perpendicular” and “valley to
555 valley” among samples. In addition, NO₃⁻ peaks were rather frequently discovered as not
556 integrated or identified; SO₄²⁻ peaks were found to have an incorrectly defined baseline due to
557 peak fronting and tailing. Adjustment of individual peak integrations was found to be difficult
558 and inefficient with features provided by MARGA tool software. Hence, an alternative
559 integration software, Chromeleon by Thermo Scientific Dionex, was used to reprocess the raw



560 chromatograms. A custom Java script was developed to incorporate MARGA raw conductivity
561 data into Chromeleon for reprocessing.

562 Though a number of chromatography issues with the MARGA commercial software were
563 identified, a relatively small percentage (6.2%) of data, overall, were invalidated due to peak
564 misintegration issues during the one-month field study described here. NO_3^- peaks appeared to be
565 the analyte most affected and higher rates of data invalidation may be expected where NO_3^-
566 concentrations are typically low. The additional flexibility and consistency of Chromeleon in
567 integrating small peaks results in lower method detection limits relative to the MARGA
568 chromatography software. Very good agreement between the two chromatography methods was
569 observed for cations across the range of observed ambient concentrations and for anions at
570 concentrations above $\sim 1\mu\text{g}/\text{m}^3$. At ambient concentrations below $\sim 1\mu\text{g}/\text{m}^3$, however,
571 concentrations determined using the MARGA software are biased +30% and +10% for NO_3^- and
572 SO_4^{2-} , respectively, compared to concentrations determined using the alternative chromatography
573 procedure. Differences between the two methods increase at lower concentrations. Over the
574 range of conditions observed in our field study, the bias in NO_3^- produces non-trivial errors in
575 average NO_3^- concentrations and metrics of particle acidity. The cause of this bias is unclear but
576 can be controlled by correcting NO_3^- and SO_4^{2-} with multi-point calibration curves rather than
577 relying solely on the MARGA LiBr internal standard.

578 During the field campaign, the MARGA captured rapid compositional changes in $\text{PM}_{2.5}$,
579 including changes in neutralization state. A particularly high NO_3^- episode associated with arctic
580 air mass intrusion and transport of pollutants from sources in the mid-west U.S. was observed.
581 Our field study demonstrates the usefulness of the MARGA system for characterizing the
582 temporal characteristics of the sulfate-nitrate-ammonium system associated with changes in local
583 (i.e., diurnal) and synoptic scale interactions between meteorology, emissions, and aerosol
584 processing.

585

586 **Acknowledgements**

587

588 We would like to acknowledge Aleksandra Djurkovic (EPA) and David Kirchgessner (EPA) for
589 laboratory and field support. We would like to acknowledge Tai Wu (EPA) for generating
590 JAVA scripts to convert MARGA data to be processed by Chromeleon. The views expressed in
591 this article are those of the authors and do not necessarily represent the views or policies of the



592 U.S. EPA. Mention of trade names does not constitute endorsement or recommendation of a
593 commercial product by U.S. EPA.

594

595 **Description of Supplemental Information**

596 Table of multi-level external standards and certified standard; table of peak areas of internal LiBr
597 standard as integrated by MARGA tool and Chromeleon for different external standard levels;
598 table of fraction of data points invalidated due to misidentification and misintegration by
599 MARGA tool; figures showing examples of misidentification and misintegration by MARGA
600 tool; figure showing comparison of Chromeleon and MARGA tool in field samples at low
601 concentrations of SO_4^{2-} and NO_3^- ; figure of corresponding back trajectories of three SO_2
602 episodes; figure of SO_2 point source emission inventory map (2011) covering mid and eastern
603 US.

604 **References**

605 Al-Horr, R., Samanta, G., and Dasgupta, P.K., 2003. A continuous analyzer for soluble anionic
606 constituents and ammonium in atmospheric particulate matter. *Environ. Sci. Tech.*, 37, 5711-
607 5720.

608

609 Allen, H.M., Draper, D.C., Ayres, B.R., Ault, A., Bondy, A., Takahama, S., Modini, R.L.,
610 Baumann, K., Edgerton, E., Knote, C., Laskin, A., Wang, B., and Fry, J.L., 2015. Influence of
611 crustal dust and sea spray supermicron particle concentrations and acidity on inorganic NO_3^- -
612 aerosol during the 2013 Southern Oxidant and Aerosol Study. *Atmos. Chem. Phys.*, 15, 10669-
613 10685.

614

615 Benedict, K.B., Chen, X., Sullivan, A.P., Li, Y., Day, D., Prenni, A.J., Levin, E.J.T.,
616 Kreidenweis, S.M., Malm, W., Schichtel, B.A., Collett, J.L., 2013. Atmospheric concentrations
617 and deposition of reactive nitrogen in Grand Teton National Park. *J. Geophys. Res.*, 118, 11875-
618 11887.

619

620 Chen, X., Day, D., Schichtel, B., Malm, W., Matzoll, A.K., Mojica, J., McDade, C.E., Hardison,
621 E.D., Hardison, D.L., Walters, S., Van De Water, M., Collett, J.L., 2014. Seasonal ambient
622 ammonia and ammonium concentrations in a pilot IMPROVE NH_x monitoring network in the
623 western United States. *Atmos. Environ.*, 91, 118-126.

624

625 Currie, L. 1999. Nomenclature in evaluation of analytical methods including detection and
626 quantification capabilities (IUPAC Recommendations 1995). *Analytica Chimica Acta.*, 391, 105-
627 126.

628



- 629 Draxler, R.R., Rolph, G.D., 2003. HYSPLIT (hybrid single particle Lagrangian integrated
630 trajectory) model access via website (<http://www.arl.noaa.gov/ready/hysplit4.html>). NOAA Air
631 Resources Laboratory, Silver Spring, MD.
632
- 633 Finlayson-Pitts, B.J., and Pitts, J.N., 2000. Chemistry of the upper and lower atmosphere.
634 Academic Press, New York, 2nd edition.
635
- 636 Huang, Y., Li, L., Li, J., Wang, X., Chen, H., Chen, J., Yang, X., Gross, D.S., Wang, H., Qiao,
637 L., and Chen, C., 2013. A case study of the highly time-resolved evolution of aerosol chemical
638 and optical properties in urban Shanghai, China. *Atmos. Chem. Phys.*, 13, 3931-3944.
639
- 640 Jayne, J.T., Leard, D.C., Zhang, X., Davidovits, P., Smith, K.A., Kolb, C.E., Worsnop, D.R.,
641 2000. Development of an Aerosol Mass Spectrometer for size and composition analysis of
642 submicron particles. *Aerosol Sci. Tech.*, 33, 49-70.
643
- 644 Khezri, B., Mo, H., Yan, Z., Chong, S-L., Heng, A.K., and Webster, R.D., 2013. Simultaneous
645 online monitoring of inorganic compounds in aerosols and gases in an industrialized area.
646 *Atmos. Environ.*, 80, 352-360.
647
- 648 Khlystov, A., Wyers, G.P., and Slanina, J., 1995. The steam-jet aerosol collector.
649 *Atmos. Environ.*, 29, 2229-2234.
650
- 651 Lee, B.P., Li, Y.J., Yu, J.Z., Louie, P.K.K., and Chan, C.K., 2013. Physical and chemical
652 characterization of ambient aerosol by HR-ToF-AMS at a suburban site in Hong Kong during
653 springtime 2011. *J. Geophys. Res.*, 118, 8625-8639.
654
- 655 Li, Y., Schichtel, B.A., Walker, J.T., Schwede, D.B., Chen, X., Lehmann, C.M.B.,
656 Puchalski, M.A., Gay, D.A., Collett, J.L., 2016. Increasing importance of deposition of reduced
657 nitrogen in the United States. *Proceedings of the National Academy of Sciences*, 113, 5874-
658 5879.
659
- 660 Markovic, M.Z., VandenBoer, T.C., and Murphy J.G., 2012. Characterization and optimization
661 of an online system for the simultaneous measurement of atmospheric water-soluble constituents
662 in the gas and particle phases. *J. Environ. Monit.*, 14, 1872-1884.
663
- 664 Makkonen, U., Virkkula, A., Mäntykenttä, J., Hakola, H., Keronen, P., Vakkari, V., and
665 Aalto, P. P., 2012. Semi-continuous gas and inorganic aerosol measurements at a Finnish urban
666 site: comparisons with filters, nitrogen in aerosol and gas phases, and aerosol acidity. *Atmos.*
667 *Chem. Phys.*, 12, 5617-5631.
668
- 669 Mensah, A.A., Holzinger R., Otjes, R., Trimborn, A., Mentel, T.F., ten Brink, H., Henzing, B.,
670 and Kiendler-Scharr, A., 2012. Aerosol chemical composition at Cabauw, The Netherlands as
671 observed in two intensive periods in May 2008 and March 2009. *Atmos. Chem. Phys.*, 12, 4723-
672 4742.
673
- 674 Phillips, G.J., Makkonen, U., Schuster G., Sobanski, N., Hakola, H., Crowley, J.N., 2013. The



- 675 detection of nocturnal N_2O_5 as HNO_3 by alkali and aqueous-denuder techniques. Atmos.
676 Meas. Tech., 6, 231-237.
677
- 678 Pinder, R.W., Adams P.J., and Pandis S.N., 2007. Ammonia emission controls as a cost-effective
679 strategy for reducing atmospheric particulate matter in the Eastern United States. Environ. Sci.
680 Technol., 41, 380-386.
681
- 682 Puchalski, M.A., Rogers, C.M., Baumgardner, R., Mishoe, K.P., Price, G., Smith, M.J., Watkins,
683 N., and Lehmann, C.M., 2015. A statistical comparison of active and passive ammonia
684 measurements collected at Clean Air Status and Trends Network (CASNET) sites. Environ Sci
685 Processes & Impacts, 17, 358-369.
686
- 687 Rumsey, I., Cowen, K., Walker, J.T., Kelley, T.J., Hanft, E.A., Mishoe, K., Rogers, C., Proost,
688 R., Beachley, G.M., Lear, G., Frelink, T., and Otjes, R.P., 2014. An assessment of the
689 performance of the Monitor for AeRosols and GAses in ambient air (MARGA): a semi-
690 continuous method for soluble compounds. Atmos. Chem. Phys., 14, 5639–5658.
691
- 692 Rumsey, I., and Walker, J.T., 2016. Application of an online ion-chromatography-based
693 instrument for gradient flux measurements of speciated nitrogen and sulfur. Atmos. Meas. Tech.,
694 9, 2581-2592.
695
- 696 Schaap, M., Otjes, R.P., and Weijers, E.P., 2011. Illustrating the benefit of using hourly
697 monitoring data on secondary inorganic aerosol and its precursors for model evaluation. Atmos.
698 Chem. Phys., 11, 11041-11053.
699
- 700 Seinfeld, J.H., and Pandis, S.N., 2006. Atmospheric Chemistry and Physics. John Wiley & Sons,
701 New York, 2nd edition.
702
- 703 Shi, Y., Chen, J., Hu, D., Wang, L., Yang, X., and Wang, X., 2014. Airborne submicron
704 particulate (PM₁) pollution in Shanghai, China: Chemical variability, formation/dissociation of
705 associated semi-volatile components and the impacts on visibility. Science of the total
706 environment, 473, 199-206.
707
- 708 Trebs, I., Meixner, F.X., Slanina, J., Otjes, R., Jongejan, P., and Andreae, M.O., 2004. Real-time
709 measurements of ammonia, acidic trace gases and water-soluble inorganic aerosol species at a
710 rural site in the Amazon Basin. Atmos. Chem. Phys., 4, 967-987.
711
- 712 Trebs, I., Andreae, M.O., Elbert, W., Mayol-Bracero, O.L., Soto-Garcia, L.L., Rudich, Y.,
713 Falkovich, A.H., Maenhaut, W., Artaxo, P., Otjes, R., and Slania, J., 2008. Aerosol inorganic
714 composition at a tropical site: discrepancies between filter-based sampling and a semi-
715 continuous method. Aerosol Sci. Tech., 42, 255-269.
716
- 717 Twigg, M.M., Di Marco, C.F., Leeson, S., van Dijk, N., Jones, M.R., Leith, I.D., Morrison, E.,
718 Coyle, M., Proost, R., Peeters, A.N.M., Lemon, E., Frelink, T., Braban, C.F., Nemitz, E., and
719 Cape, J.N., 2015. Water soluble aerosols and gases at a UK background site-Part 1: Controls of
720 PM_{2.5} and PM₁₀ aerosol composition. Atmos. Chem. Phys., 15, 8131-8145.



- 721
722 U.S. Environmental Protection Agency (U.S. EPA), 2011. Environmental Technology
723 Verification report: Applikon MARGA semi-continuous ambient air monitoring system. U.S.
724 EPA, Office of Research and Development. EPA/600/R111106VR.
- 725 van Os, M.J., Slanina, J., de Ligny, C.L., and Agterdenbos, J. 1984. Linear calibration in ion
726 chromatography by calculating total amounts of sample from measured conductivity data. Anal.
727 Chim. Acta, 156, 169-180.
- 728 Vayenas, D.V., Takahama, S., Davidson, C., Pandis, S.N., 2005. Simulation of the
729 thermodynamic and removal processes in the sulfate-ammonia-nitric acid system during winter:
730 Implication for PM_{2.5} control strategies. J. Geophys. Res., 110, DOI:10.1029/2004JD005038.
731
- 732 Weber, R.J., Orini, D., Daun, Y., Lee, Y-N., Klotz, P.J., and Brechtel, F., 2001. A Particle-into-
733 Liquid collector for rapid measurement of aerosol bulk chemical composition. Aerosol Sci.
734 Tech., 35, 718-727.
735
- 736 Weber, R., Orsini, D., Duan, Y., Baumann, K., Kiang, C.S., Chameides, W., Lee, Y.N., Brechtel,
737 F., Klotz, P., Jongejan, P., ten Brink, H., Slanina, J., Boring, C.B., Genfa, Z., Dasgupta, P.,
738 Hering, S., Stolzenburg, M., Dutcher, D.D., Edgerton, E., Hartsell, B., Solomon, P., and Tanner,
739 R., 2003. Intercomparison of near real time monitors of PM_{2.5} nitrate and sulfate at the U.S.
740 Environmental Protection Agency Atlanta Supersite. J. Geophys. Res., 108, 8421,
741 doi:10.1029/2001JD001220.
742
- 743 Wolff, V., Trebs, I., Ammann, C., Meixner, F.X. 2010. Aerodynamic gradient measurements of
744 the NH₃-HNO₃-NH₄NO₃ triad using a wet chemical instrument: an analysis of precision
745 requirements and flux errors. Atmos. Meas. Tech., 3, 187-208.
746
- 747 Wyers, G.P., Otjes, R.P., and Slanina J., 1993. A continuous-flow denuder for the measurement
748 of ambient concentrations and surface-exchange fluxes of ammonia. Atmos. Environ., 27, 2085-
749 2090.
750
751



752 **Tables**

753 Table 1. Method detection limits for chromatograms processed by MARGA tool and re-
754 integrated by Chromeleon.

	Chromeleon		MARGA tool	
	MDL($\mu\text{g}/\text{m}^3$)	# of sample	MDL($\mu\text{g}/\text{m}^3$)	# of sample
NH_4^+	0.02	78	0.04	78
NH_3	0.02	78	0.04	78
SO_4^{2-}	0.08	80	0.13	76
SO_2	0.05	80	0.08	76
NO_3^-	0.08	80	0.14	76
HNO_3	0.08	80	0.14	76

755

756

757

758

759

760

761

762

763

764

765

766

767

768

769

770



771 Table 2. Comparison between MARGA sample boxes 1 and 2 for particulate NO_3^- , SO_4^{2-} and
 772 NH_4^+ , gas phase HNO_3 , SO_2 and NH_3 by orthogonal least squares regression. N is number of
 773 observations, C_{average} is average air concentration, $\sigma_{\Delta C}$ is the standard deviation of the orthogonal
 774 least squares residuals (i.e., detection limit (DL)), $\sigma_{\Delta C}/C_{\text{avg}}$ is the precision estimate, C_{max} and
 775 C_{min} are the maximum and minimum air concentrations, respectively. Percentage of observations
 776 below the detection limit (DL) is also included.

	Slope	Intercept	$\sigma_{\Delta C}$ $\mu\text{g}/\text{m}^3$	N	C_{average} $\mu\text{g}/\text{m}^3$	C_{max} $\mu\text{g}/\text{m}^3$	C_{min} $\mu\text{g}/\text{m}^3$	$\sigma_{\Delta C}/C_{\text{avg}}$ %	<DL%
NH_4^+	0.98	0.01	0.02	616	0.52	2.20	0.10	4	0
NH_3	1.02	-0.03	0.03	614	0.33	1.62	0	9	5
SO_4^{2-}	0.99	0.01	0.05	602	1.41	4.39	0.17	4	0
SO_2	0.96	0.02	0.15	603	0.98	23.26	-0.01	15	27
NO_3^-	1.00	0.00	0.01	602	0.21	3.18	0	5	17
HNO_3	0.83	0.01	0.03	603	0.19	0.97	0	16	20

777

778



779 Table 3. Summary of concentrations ($\mu\text{g}/\text{m}^3$) of aerosol and precursor gases during and outside
780 of cold air mass periods.

	Cold Event			Non-Cold event		
	Average	Median	Max	Average	Median	Max
NH ₃	0.12	0.09	0.29	0.35	0.24	1.62
HNO ₃	0.35	0.30	0.82	0.17	0.13	0.97
SO ₂	3.22	1.32	32.56	0.73	0.42	8.09
NH ₄ ⁺	0.99	0.88	2.20	0.48	0.45	1.21
NO ₃ ⁻	1.07	0.72	3.18	0.13	0.09	0.98
SO ₄ ²⁻	1.93	1.66	4.39	1.33	1.29	3.58
Temperature	4.54	5.00	13.9	12.88	12.20	29.40
RH	50	51	77	70	71	100

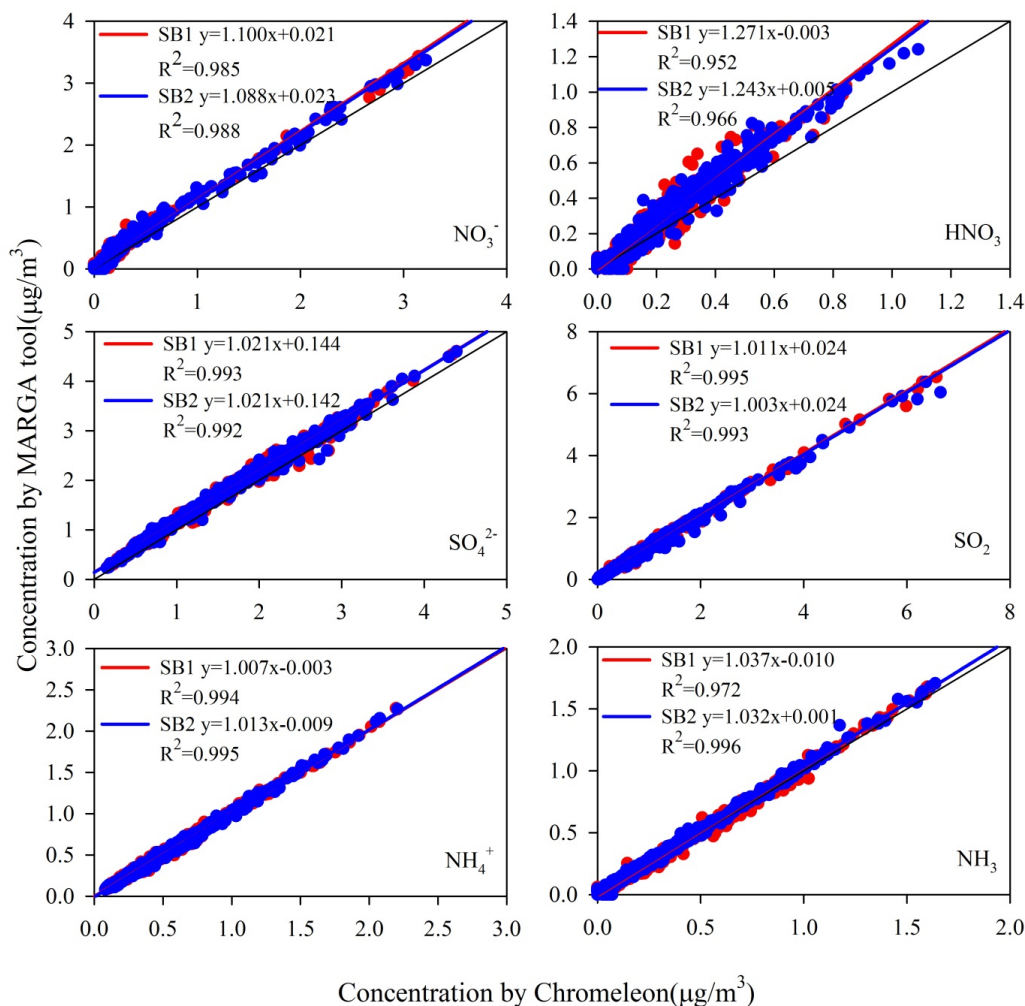
781

782

783



784 **Figures**



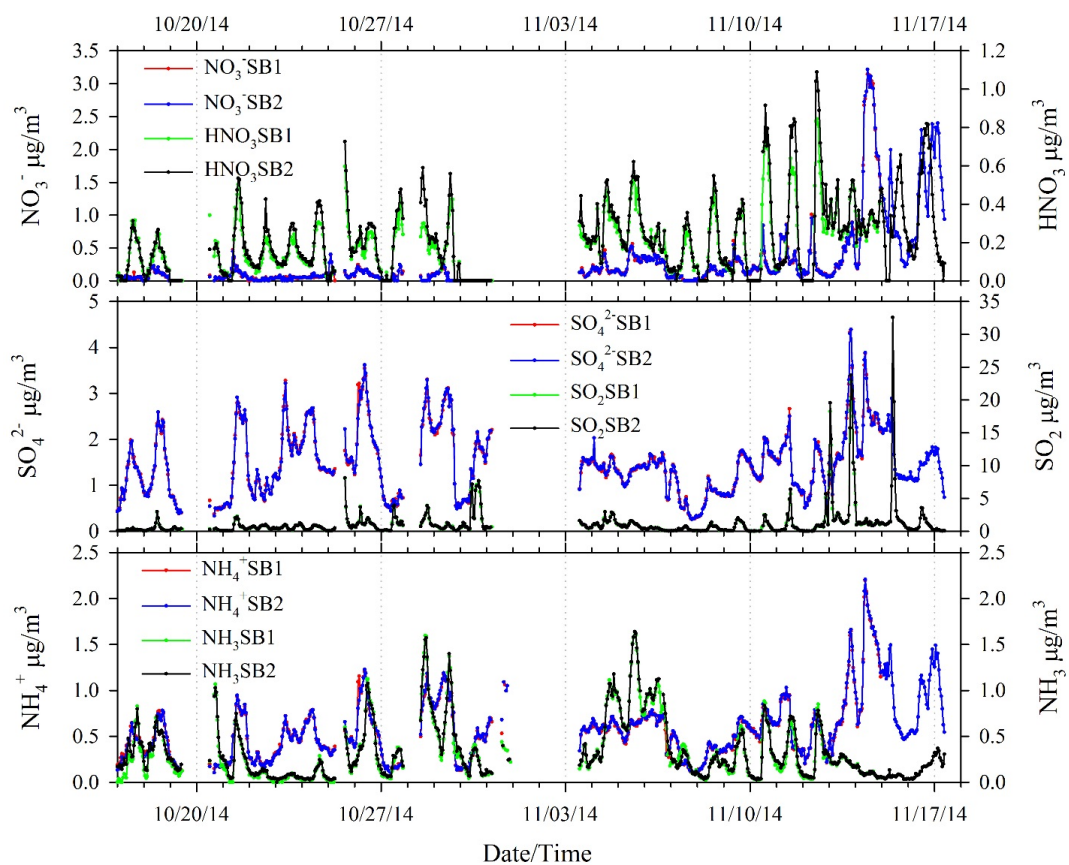
785

786 Figure 1. Comparison of concentrations of analytes monitored during fall of 2014 at Duke Forest
 787 as reported by MARGA tool and Chromeleon. Data points with misintegration issues by
 788 MARGA tool were excluded from this comparison. Data for individual sample boxes (SB1 and
 789 SB2) are shown.

790

791

792



793

794 Figure 2. Time series of concentrations of particulate NO_3^- , SO_4^{2-} and NH_4^+ , gas phase HNO_3 ,
795 SO_2 and NH_3 by collocated MARGA sample boxes 1 (SB1) and 2 (SB2).

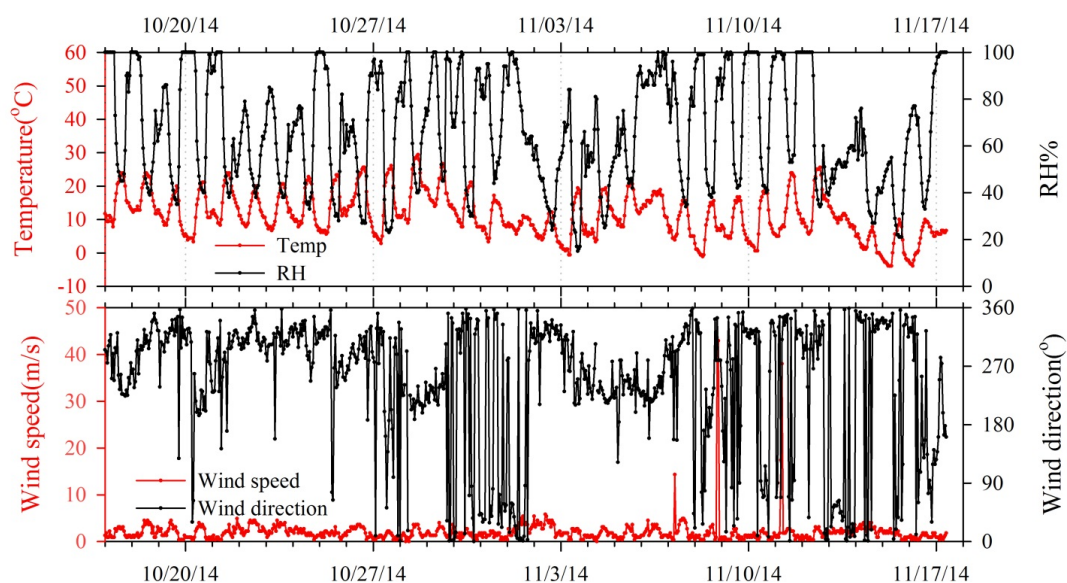
796

797

798

799

800



801

802 Figure 3. Hourly temperature, relative humidity, wind speed and wind direction during the fall
803 2014 field intensive.

804

805

806

807

808

809

810

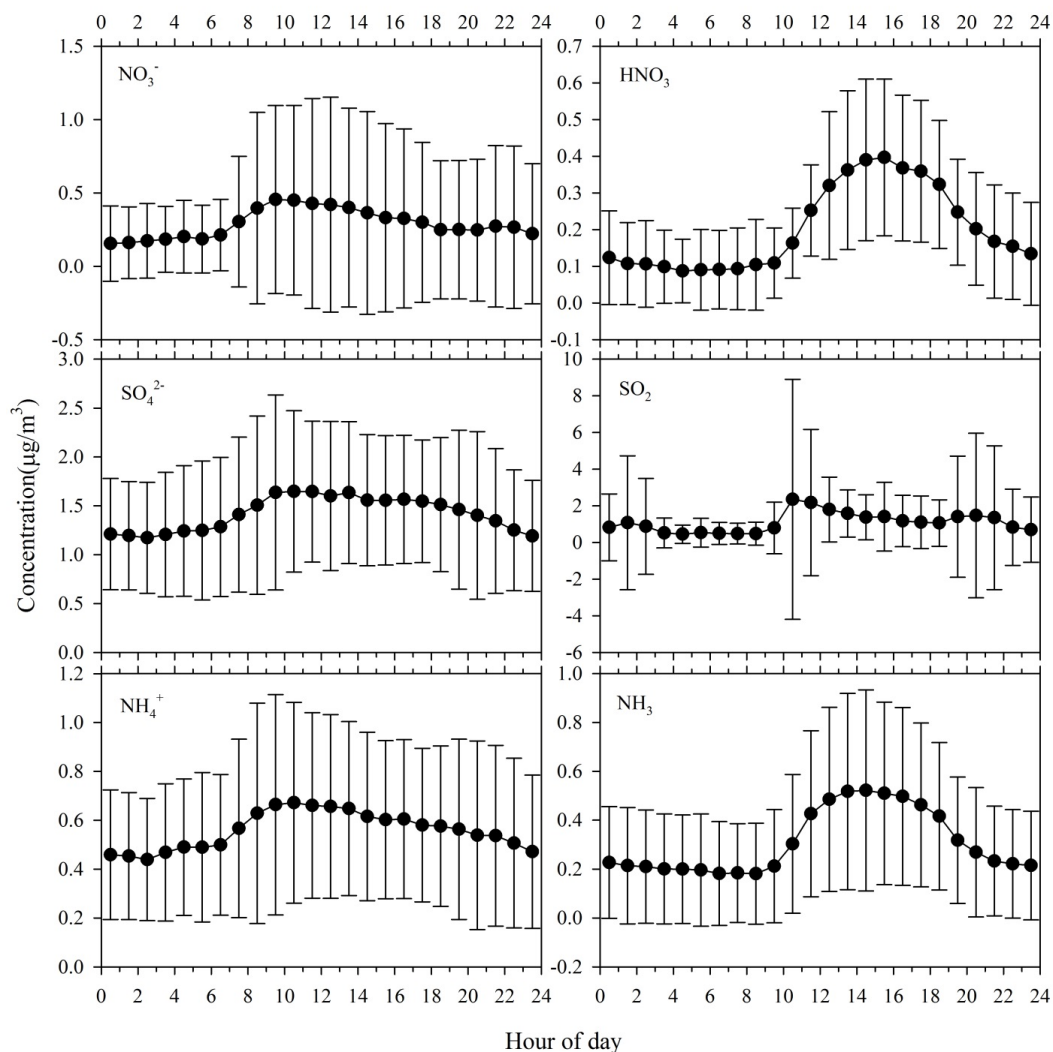
811

812

813

814

815



816

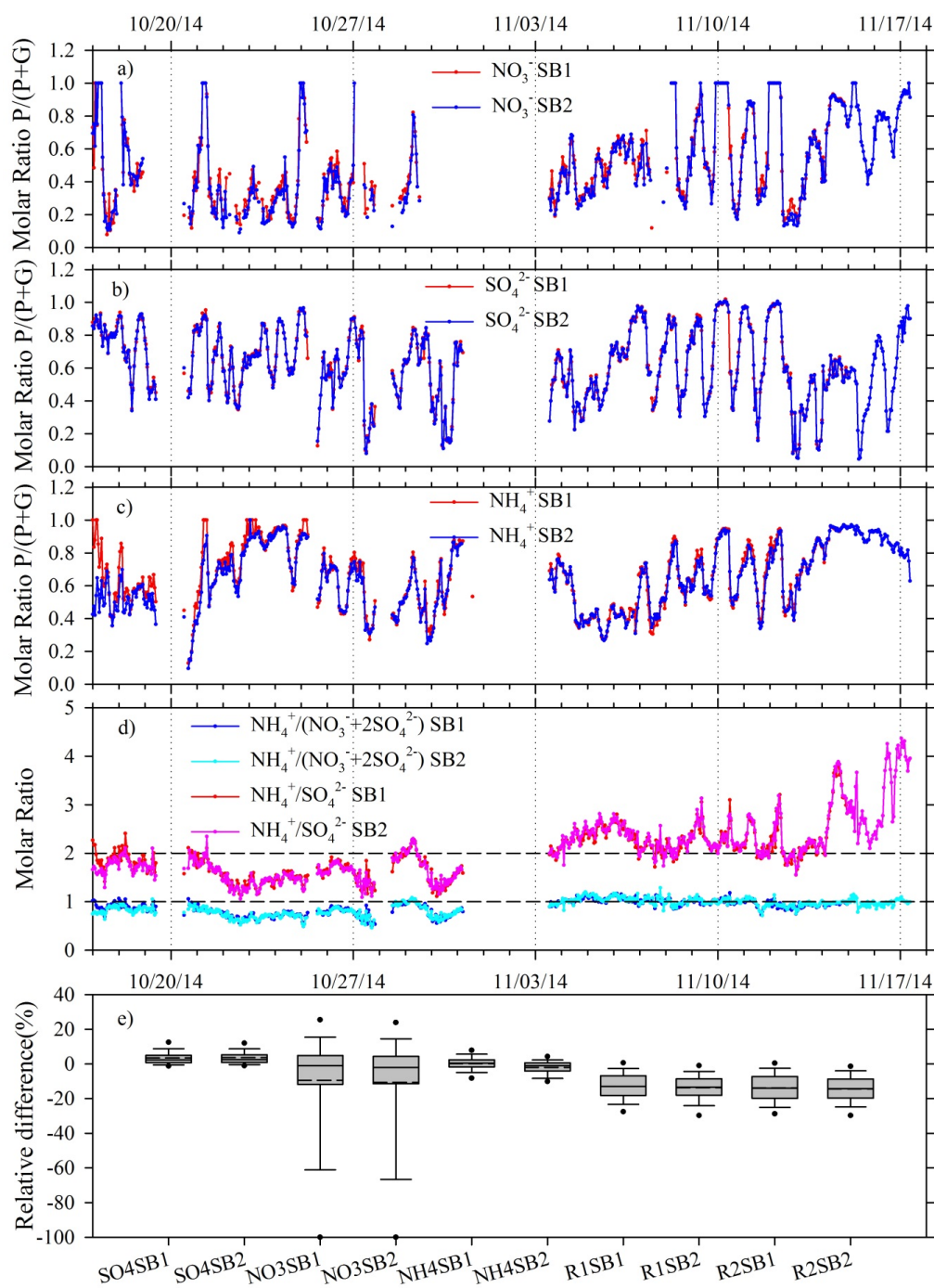
817 Figure 4. Diurnal profiles of particulate NO_3^- , SO_4^{2-} and NH_4^+ , gas phase HNO_3 , SO_2 and NH_3
818 during the fall 2014 field intensive. Data points represent average concentrations, while error
819 bars represent 1 standard deviation.

820

821

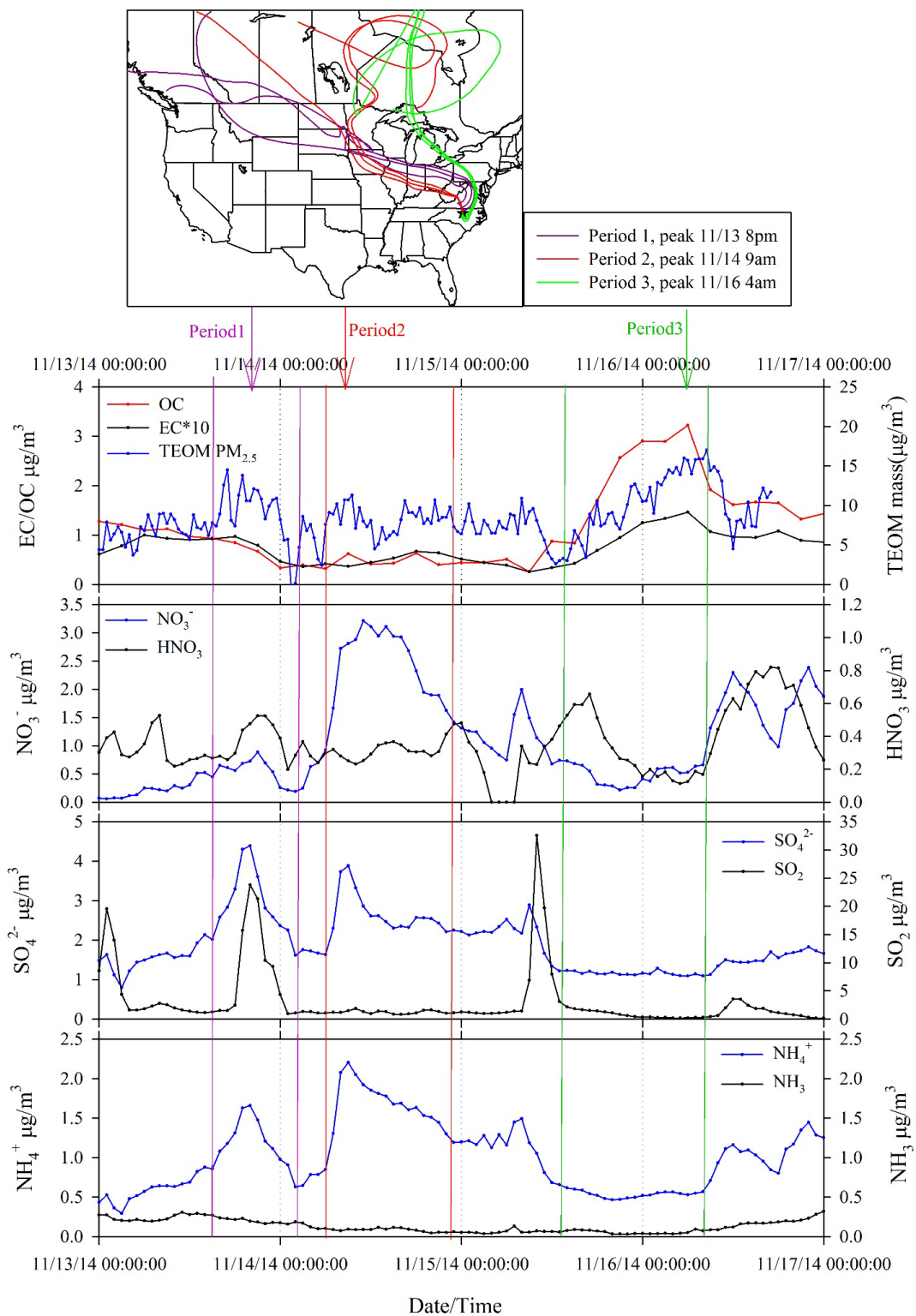
822

823





825 Figure 5. Partitioning molar ratios of a) NO_3^- , b) SO_4^{2-} and c) NH_4^+ in particle phase, calculated
826 as particle/(particle+gas); d) molar ratios (R1 and R2) of particulate NO_3^- , SO_4^{2-} and NH_4^+ to
827 determine particle neutralization state and acidity; e) relative difference of partitioning molar
828 ratios of NO_3^- , SO_4^{2-} and NH_4^+ in particle phase as well as particle neutralization state indicators
829 R1 and R2 by Chromeleon and MARGA tool. Negative values indicate a lower ratio calculated
830 by the MARGA tool (i.e., positive bias in concentrations calculated by MARGA tool). Solid and
831 dash lines inside box represent median and mean, respectively. Top and bottom box represent
832 75th and 25th percentiles. Whiskers represent 90th and 10th percentiles. Dots represent 95th and 5th
833 percentiles. SB1 and SB2 indicate collocated MARGA sample boxes 1 and 2, respectively.





835 Figure 6. High concentration periods observed during mid-November 2014. Period 1: highest
836 SO_4^{2-} ; Period 2: highest NH_4^+ and NO_3^- ; Period 3: highest OC. Corresponding back trajectories
837 (arrival at 500AGL, backwards for 168hrs) of individual period peaks (± 2 hrs) are also presented.

838

839

840

841

842

843

844

845

846

847

848

849

850

851

852

853

854

855

856

857

858